Comparison of Precipitation Derived from the ECMWF Operational Forecast Model and Satellite Precipitation Datasets

CHRIS KIDD

Earth System Science Interdisciplinary Center, University of Maryland, College Park, College Park, and NASA Goddard Space Flight Center, Greenbelt, Maryland

ERIN DAWKINS

School of Earth and Environment, University of Leeds, Leeds, United Kingdom

GEORGE HUFFMAN

NASA Goddard Space Flight Center, Greenbelt, Maryland

(Manuscript received 17 December 2012, in final form 25 April 2013)

ABSTRACT

Precipitation is an important component of the climate system, and the accurate representation of the diurnal rainfall cycle is a key test of model performance. Although the modeling of precipitation in the cooler midlatitudes has improved, in the tropics substantial errors still occur. Precipitation from the operational ECMWF forecast model is compared with satellite-derived products from the Tropical Rainfall Measuring Mission (TRMM) Multisatellite Precipitation Analysis (TMPA) and TRMM Precipitation Radar (PR) to assess the mean annual and seasonal diurnal rainfall cycles. The analysis encompasses the global tropics and subtropics (40°N–40°S) over a 7-yr period from 2004 to 2011. The primary aim of the paper is to evaluate the ability of an operational numerical model and satellite products to retrieve subdaily rainfall. It was found that during the first half of the analysis period the ECMWF model overestimated precipitation by up to 15% in the tropics, although after the implementation of a new convective parameterization in November 2007 this bias fell to about 4%. The ECMWF model poorly represented the diurnal cycle, simulating rainfall too early compared to the TMPA and TRMM PR products; the model simulation of precipitation was particularly poor over Indonesia. In addition, the model did not appear to simulate mountain-slope breezes well or adequately capture many of the characteristics of mesoscale convective systems. The work highlights areas for further study to improve the representation of subgrid-scale processes in parameterization schemes and improvements in model resolution. In particular, the proper representation of subdaily precipitation in models is critical for hydrological modeling and flow forecasting.

1. Introduction

Precipitation varies greatly in both time and space, particularly at fine spatial and temporal scales (Michaelides et al. 2009). The diurnal rainfall cycle represents one of the most fundamental modes of variability in the global climate system as a result of the well-defined variations in solar forcing, changes in the radiation budget, and their influence on precipitation processes (Yang and Slingo 2001; Wang et al. 2007). Although the modeling of precipitation is reasonably accurate for the cooler midlatitudes in which large-scale synoptic patterns are common (Kidd et al. 2012), modeling skill decreases over the tropics where convective systems dominate. Here processes governing precipitation are typically at finer spatial and temporal scales (Huffman et al. 2010), and the ability of the models to capture these finer spatiotemporal precipitation characteristics remains one of the critical unresolved issues in climatology (Michaelides et al. 2009).

As a forced component of the climate system and as a result of complex interactions among topographical features, differential surface heating, and land–sea contrasts, the ability of a model to accurately reproduce the observed diurnal rainfall cycle variability serves as

Corresponding author address: Chris Kidd, NASA Goddard Space Flight, Mail Code 612, Greenbelt, MD, 20771.
E-mail: chris.kidd@nasa.gov

DOI: 10.1175/JHM-D-12-0182.1

© 2013 American Meteorological Society

a test of model performance (Bell and Reid 1993; Vondou et al. 2010). This is particularly important with the parameterization of subgrid-scale processes. While a large number of studies have focused on how well a model simulates the regional diurnal rainfall cycles (Dai et al. 1999; Negri et al. 2002; de Angelis et al. 2004; Sanderson et al. 2006; Kikuchi and Wang 2008; Laing et al. 2008; Liu et al. 2009; Takahashi et al. 2010), few have examined how well a high-resolution model performs across the whole of the global tropics. In this study a comparison is made between a high-resolution numerical weather prediction model, a gauge-scaled merged satellite product, and a satellite precipitation radar product.

This paper assesses how well the operational European Centre for Medium-Range Weather Forecasts (ECMWF) forecast model simulates the mean annual and seasonal diurnal rainfall cycles relative to the satellite-derived Tropical Rainfall Measuring Mission (TRMM) Merged Precipitation Analysis (TMPA) and Precipitation Radar (PR) products across the global tropics (40°N–40°S 180°W–180°E) over a 7-yr time period (2004–11). This is the region where models typically show the least accuracy at simulating precipitation compared to observational results because of precipitation being strongly modulated by local factors, such as differential diurnal surface heating and moisture availability (Laing et al. 2008).

The background to the study is reviewed in section 2, while section 3 provides information on the ECMWF model, TMPA, and TRMM PR datasets, as well as a description of the methodology used. Section 4 presents the results of the study, which are discussed in detail in section 5. Finally, section 6 provides a summary of the study.

2. Background

a. The observation of precipitation

The accurate measurement and monitoring of precipitation is crucial to a range of applications, including the assessment of the accuracy of regional and large-scale climate simulations (Meehl et al. 2007; Allan et al. 2010). The two main sources of precipitation observation data are (i) surface gauge measurements and (ii) estimates from satellite remote sensing. While surface gauge measurements represent the "ground truth," they have limited global coverage, being mostly restricted to land surfaces in developed regions, with ocean coverage only available from very sparse island, buoy, and ship-borne gauges. Only 25% of the Earth's surface can be considered to have adequate coverage from gauge-derived precipitation measurements (New et al. 2001). In addition, these gauges represent point sources and may be subject to measurement issues caused by local effects such as topography or wind-induced undercatch.

Satellite-borne sensors can provide complete coverage at a range of spatiotemporal scales dependent upon the specific sensor used (Kidd et al. 2009; Kidd and Levizzani 2011). As such, they play a key role in estimating precipitation over the oceans and over remote land areas where few or no ground-truth measurements exist, thus providing a "best available" estimate of precipitation (Kidd and Huffman 2011). The longest-available set of observations useful for precipitation studies are those from infrared (IR) sensors. These observations are available at relatively high resolutions (1–4 km) with temporal samples as frequent as every 15 min. However, since IR techniques are based on cloud top characteristics, they are also the most indirect measure of precipitation at the surface. Well-calibrated passive microwave (PMW) observations have been available since mid-1987 and provide a more direct measure of precipitation, although at the expense of temporal sampling. The most direct measurements are available from spaceborne precipitation radar that has been available since 1997; however, it is limited to a single satellite sensor with very limited swath coverage.

The highly variable nature of precipitation, the infrequent and discontinuous nature of the satellite observations, and regional and temporal biases shown by individual satellite algorithms mean that sampling errors are introduced in these estimates relative to the ground-truth values from the surface gauges (e.g., Nesbitt and Anders 2009). It has therefore been the goal of precipitation algorithm developers to combine information from sensors with good temporal and spatial resolutions (with less direct measures) with those with more direct measures of precipitation (with poorer sampling). Such techniques include the TMPA technique (Huffman et al. 2010), the National Oceanic and Atmospheric Administration (NOAA) Climate Prediction Center morphing technique (CMORPH; Joyce et al. 2004) and the Global Satellite Mapping of Precipitation technique (GSMaP; Aonashi et al. 2009).

b. Model parameterization

Because of limitations in computing power and the understanding of certain physical processes, a model can represent only part of the actual Earth system (McGuffie and Henderson-Sellers 2005). Computing power is a major limiting factor in weather and climate models, which calculate the physical state of the atmosphere across a three-dimensional grid spanning the Earth's surface. This grid resolution is important in determining the ability of the model to more closely represent reality. However, computational costs are extremely

large at higher resolutions (Kalnay 2003). As such, a trade-off must be sought between grid resolution and computation time, so that model physics can be computed within an appropriate time frame (Trenberth 1991). Importantly, many physical processes occur at smaller scales than the size of the individual grid boxes. These subgrid-scale physical processes, including condensation, evaporation, turbulent transfers of moisture, and others for which the physics are not fully understood, can be included in a model via parameterization (parametric representation). This parameterization approximates unresolved physical processes based on the knowledge of processes explicitly resolved by the model (e.g., Kalnay 2003).

Precipitation itself is a function of the available atmospheric moisture and the convergence of that moisture and is parameterized in a model through (i) the gross condensation (entrainment minus detrainment) rate, (ii) latent heat energy exchange within the atmosphere, and (iii) the microphysical behavior of clouds (McGuffie and Henderson-Sellers 2005). Clouds play an important role in the radiative budget of Earth as well as in the hydrological cycle. However, individual clouds typically occur at subgrid scales and must be collectively parameterized based on resolved variables, such as average humidity and temperature (Trenberth 1991). It is assumed that the average humidity and temperature calculated by a model for a grid box using resolved physics can be used to calculate the average cloudiness for that grid box. The parameterization of cloud, and thus precipitation, processes continues to be one of the greatest sources of uncertainty in numerical weather prediction (NWP) and climate models (Tompkins and Di Giuseppe 2010).

c. *The diurnal rainfall cycle*

Within the tropics the annual and seasonal distributions of rainfall are heavily influenced by the migration of the intertropical convergence zone (ITCZ) northward and southward throughout the year, in phase with the solar insolation cycle (Bridgman and Oliver 2006; Liu et al. 2009) as well as by the monsoonal regimes (Peixoto and Oort 1992). Rainfall maxima typically occur along the ITCZ and the South Pacific convergence zone (SPCZ) regions and over equatorial land areas. Minima typically occur over the subtropical high pressure cells, particularly over northern Africa and in the southeast Pacific and Atlantic oceans. However, within these regions lie complex subdaily patterns of rainfall driven by the availability of moisture and solar forcing.

The diurnal cycle, along with the seasonal cycle, represents the most fundamental modes of variability in the global climate system. These cycles are associated with the well-defined variations in solar forcing (Wang et al. 2007; Vondou et al. 2010) and the resultant change in the incoming and outgoing radiative budget.

Satellite and surface observations demonstrate that rainfall can have a significant diurnal cycle (24-h period), with the amplitude of the cycle over land greater than that of the open oceans (Gray and Jacobsen 1977). Over most land areas, observations indicate that there is a late afternoon/early evening rainfall maximum (Liu et al. 2009) with a mean-to-peak amplitude of 30%–125% of the daily mean in precipitation amount in summer. An early morning maxima is well documented over the open oceans, with a mean-to-peak amplitude of 10%–30% and a late afternoon minimum (Dai et al. 2007; Takahashi et al. 2010; Yang and Slingo 2001; Nesbitt and Zipser 2003). In addition, there is evidence of a weak semidiurnal rainfall cycle occurring every 12 h with a peak around 0300 LST (local solar time) in the tropics (Dai et al. 2007). The diurnal rainfall cycle tends to be the most pronounced over regions of intense convective activity such as over the ITCZ, in the equatorial regions of western and central Africa and South America, and over Indonesia (Bechtold et al. 2004).

The differences in the observed rainfall maxima over open oceans (early morning) and over land (late afternoon–early evening) suggest very different causal mechanisms for the diurnal variation over continental and oceanic areas; an extensive review can be found in Yang and Smith (2005). The mechanisms of the late afternoon rainfall maximum are well understood and observed (Nesbitt and Zipser 2003; Kikuchi and Wang 2008) and are a response to surface heating throughout the daytime. Regional differences in the amplitude and character of the diurnal cycle may occur over land and coastal areas because of modifications by (i) local orography; (ii) local effects such as land–sea breeze circulations; (iii) the initiation, propagation, and decay of mesoscale convective systems (MCSs); and (iv) the long nocturnal life cycles of such systems (Yang and Slingo 2001; Nesbitt and Zipser 2003). For example, MCSs may preferentially occur on the leeside of mountains where the nocturnal environment provides little inhibition to the formation and downwind propagation of such systems (Dai et al. 2007).

Over the oceans the well-observed occurrence of the early morning rainfall maximum is more complex and may be the result of a number of causal mechanisms. There is evidence that this diurnal nighttime maximum over the oceans is caused by a direct radiation–convection interaction (Liu and Moncrieff 1998). The nighttime instability and enhanced convective activity is produced as a result of the radiative cooling at the cloud tops being greater than that at the cloud base leading to greater cloud development in the early morning. Similarly,

during the daytime, radiative warming at the cloud top due to solar radiation will produce increased stability and restricted convective activity leading to a late afternoon rainfall minimum over the open oceans (Yang and Slingo 2001).

With the diurnal rainfall cycle being a basic solar forced mode of the climate system, the accurate representation of this cycle therefore reflects the capability of the physical parameterizations of convective processes in a model. Most current atmospheric models do not adequately model the diurnal cycle of rainfall and often simulate unrealistically large diurnal ranges, particularly over land areas (Lee et al. 2007; Shin et al. 2007; Wang et al. 2007). Furthermore, the models often exhibit significant biases in their simulations, frequently poorly representing the diurnal rainfall cycle over land, simulating maximal rainfall too early, and/or simulating too little nighttime precipitation (Bechtold et al. 2004).

Studies have shown that the convection parameterization scheme employed and the resolution are the most crucial factors in determining how well a model represents the diurnal rainfall cycle (Shin et al. 2007). The convection parameterizations in models commonly fail to adequately resolve convective processes related to entrainment minus detrainment rates for deep convection (Bechtold et al. 2004; Wang et al. 2007) and those associated with MCSs. This is because of an incomplete representation of the effects of local topography, land surface fluxes, and their influence on convective processes (Nesbitt and Zipser 2003).

Observational datasets provide an excellent way to evaluate how well a model can represent diurnal rainfall variability. While previous studies (Ebert et al. 2007; Liu et al. 2009; Vondou et al. 2010) have tended to evaluate model performance on a regional, daily scale, few have assessed how well a high-resolution model performs across the global tropics. This study compares the ECMWF forecast model with high-quality satellite products at a 3-hourly, 0.25° × 0.25° resolution across the global tropics to provide insights into where the model–satellite systematically differ and possible causal mechanisms for this.

3. Methodology

The data used in this study are the ECMWF operational forecast model, the TMPA product, and the TRMM PR product from March 2004 to February 2011. This 7-yr period was chosen to provide a relatively robust indication of the mean annual and seasonal diurnal cycles. In addition, the datasets were readily available for this time period. Each of these datasets (summarized in Table 1) have been mapped (see below) to a spatial resolution of 0.25° × 0.25° every 3 h (the best resolution available for the TMPA product), covering the tropical region from 180°W to 180°E and from 40°N to 40°S.

TABLE 1. Summary of datasets in the comparison.

Datasets: March 2004 through February 2011
ECMWF operational forecast model:
1 Mar 2004 to 1 Feb 2006: T511L60 model (c.39-km resolution, 60 levels).
2 Feb 2006 to 26 Jan 2010: T799L91 model (25-km resolution, 91 levels).
27 Jan 2010 to 28 Feb 2011: T1279L91 model (c15.6-km resolution, 91 levels).
November 2007: Major change of convection parameterization scheme.
November 2010: New cloud scheme improving rain–snow advection.
TRMM Merged Precipitation Analysis:
Multisatellite inputs with changes in individual satellite sensors.
Bias corrected against surface gauge data on a monthly basis.
Nominal resolution of 0.25 × 0.25°, 3-hourly periods.
TRMM Precipitation Radar (2A25 product):
Near-surface rainfall product used.
Instantaneous "snapshots" aggregated into 3-hourly accumulations.
Nominal resolution of 5 km, remapped to 0.25 × 0.25° resolution.
No data between 29 May 2009 and 18 June 2009.

a. Datasets

1) TRMM PR

The TRMM 2A25 precipitation product (version 7) is derived from the TRMM PR. Launched in 1997, TRMM is a joint collaboration between the National Aeronautics and Space Administration (NASA) and the Japanese Aerospace Exploration Agency (JAXA; formerly NASDA). Its aims are to monitor and improve understanding of precipitation structure, rate, and distribution of rain across the global tropics (Kummerow et al. 1998). The TRMM satellite carries a number of instruments aimed at the observation and measurement of precipitation. In particular, the PR is the first spaceborne radar system designed to measure precipitation. It operates at a frequency of 13 GHz, provides 80 range bins with 250 m vertical resolution, and has a nominal (post 24 August 2001) resolution of 5 km at nadir. Because of the non-sun-synchronous nature of TRMM's orbit, the sensor is able to capture the diurnal nature of precipitation. However, the 247-km swath width of the PR provides a relatively poor temporal sampling and, consequently, longer observational periods are required to provide an adequate number of samples.

The basis of the 2A25 algorithm is described by Iguchi and Meneghini (1994) and takes into account the rain attenuation, scattering cross section, and height of the

freezing level; the main source of uncertainty relates to the effects of the rainfall attenuation, beam-filling effects, and surface clutter (Iguchi et al. 2009). The instantaneous near-surface precipitation estimates are mapped to the 0.25° × 0.25° grid to generate monthly accumulations of precipitation for each of the 3-hourly periods.

2) TMPA

The TMPA product (or 3B42), version 7, is a merged high-quality microwave–IR precipitation product. The first reprocessed version of the TMPA includes microwave estimates derived from a number of sensors [e.g., TRMM Microwave Imager (TMI), Special Sensor Microwave Imager (SSM/I), Special Sensor Microwave Imager/Sounder (SSM/IS), and Advanced Microwave Scanning Radiometer (AMSR)], which are optimally combined and calibrated and used to calibrate IR precipitation estimates, and they are then used to fill gaps between the passive microwave observations. Surface gauge data are used to rescale to product on a monthly basis. A detailed description of the evolution of the product can be found in Huffman et al. (2010). Precipitation estimates are available at 0.25° × 0.25° and 3-hourly resolution at the synoptic observation times of 0000, 0300, and 2100 UTC. The data for each time are centered at the nominal time ±90 min, with 0000 UTC corresponding to the period between 2230 UTC the previous day to 0130 UTC on the current day. The high spatiotemporal resolution provides an opportunity for detailed assessment of diurnal rainfall cycle.

The quality of the precipitation estimates is highly sensitive to the quality of the input precipitation estimates. As such, in some coastal regions, the occurrence and amount of precipitation may be underestimated, while these may be overestimated in arid coastal areas that are adjacent to oceans and lakes. In addition, rainfall is typically underestimated in regions of complex topography because of sparser surface gauge coverage at the higher elevations. Because of radiometric surface background effects, the occurrence of precipitation over land may be underestimated in some regions as a result of satellite schemes missing light precipitation as well as orographic precipitation over mountains. The occurrence of precipitation in the IR-based estimates used in the final TMPA product may lag behind the occurrence in the in situ rain gauge measurements (Kubota and Nitta 2001; Kikuchi and Wang 2008).

3) ECMWF MODEL

The ECMWF operational model versions used in this analysis are the T511L60, T799L91, and T1279L91 and are outlined in Table 1. This model consists of six basic physical equations, namely, two diagnostic equations (the gas law and the hydrostatic equation) and four prognostic equations (equations of continuity and motion, thermodynamic equation, and conservation of moisture), and a number of additional prognostic equations for cloud fraction, water and ice content, and ozone. All other physical processes, including the formation of clouds and precipitation, are included via parameterization. The model contains orographic information, such as fractional land area, fractional cover of vegetation type, and mean elevation above mean sea level.

The model includes both convective and stratiform precipitation via parameterization; convective precipitation forms within an updraft if the amount of condensate exceeds the amount that can be sustained by the upward velocity. If this condensate is at or above 0°C, it is defined as being water. If at a lower temperature, it is defined as snow or a mixture of snow and ice. The convection schemes calculate the vertical transport of moisture and momentum and changes in temperature associated with releases of latent heat or evaporation, in addition to distinguishing between deep, shallow, and midlevel convection.

Some known issues relate to the representation of subgrid-scale processes, in particular sea breeze penetration over inland regions. Sea breezes are typically too large and too organized to be included in the model via parameterization yet still occur at subgrid scales. As a result, the model may overestimate the extent of the sea breeze. Similar effects are also seen with wind systems near heated elevated regions. While the mean model orography can generally provide a realistic description over most of the land areas, it cannot easily resolve regions of high subgrid-scale orographic variation, such as in high mountainous areas.

Descriptions of the ECMWF precipitation schemes and performance are summarized in Moreau et al. (2003), Mahfouf et al. (2005), Bauer et al. (2005), and Kelly et al. (2008). In particular, a major change in convection parameterization occurred in November 2007; this and other improvements in the physical parameterizations within the ECMWF model are described by Jung et al. (2010).

b. *Processing*

Data for the study were collected and preprocessed to permit a direct comparison between the different precipitation products. During the period of 2004–11, the ECMWF operational forecast output was provided at three different spatial resolutions using the N256, the N400, and the N640 Gaussian grids (see Table 1). The ECMWF data were mapped to the 0.25° resolution at each of the available 3-h time steps from 0–3 h through to 45–48 h; the second 24-h forecast period was included

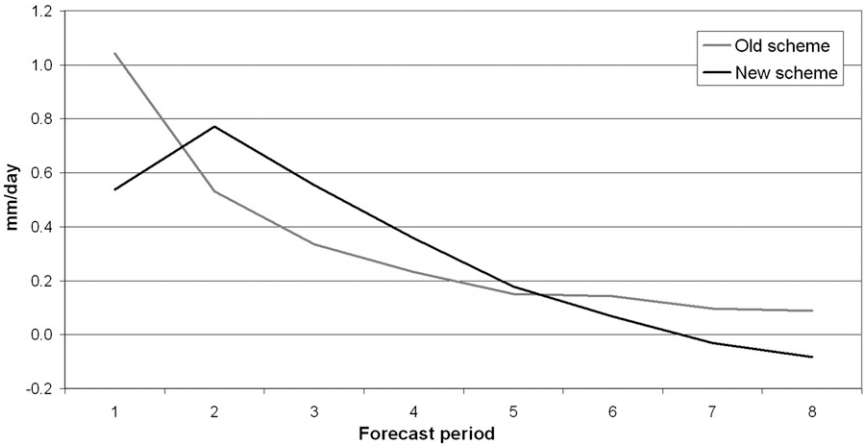

FIG. 1. Difference (mm day^{-1}) between the initial 0–24-h forecast and the subsequent 24–48-h forecast; forecast period 1 represents 0–3 minus 24–27 h, period 2 represents 3–6 minus 27–30, etc. Data covering the period from March 2004 to February 2007 under the old convection scheme are shown in gray, while the period from March 2008 to February 2011 under the new convection scheme are shown in black.

to assess the spindown period of the model. The TRMM PR data are available at the footprint resolution of the sensor, that is, latitude/longitude and instantaneous near-surface precipitation estimate; the data were mapped to the 0.25° resolution for each 3-h period over the 7 yr. The TMPA data were obtained at their native resolution of 0.25° × 0.25°, 3-hourly periods.

After preprocessing, all data were available over 1440 × 320 grid points, equivalent to 180°W–180°E and 40°N–40°S at a spatial resolution of 0.25° × 0.25° and for nominal accumulation periods every 3 h from 0000–0300 to 2100–2400 UTC. All years were defined as March to February of the following year inclusive, such that 2004 is regarded as beginning on 1 March 2004 to 28 February 2005, etc., to allow the seasonal analysis to run from March–May (MAM) to December–February (DJF). The TMPA data are available every 3 h at observation times of 0000 to 2100 UTC ±90 min. Therefore, there is a slight time offset of 1.5 h between the ECMWF and TRMM PR products and the TMPA product; the TMPA 0000 UTC was compared to ECMWF 0000–0300 UTC, TMPA 0300 UTC was compared to ECMWF 0300–0600 UTC, etc.

After initial collection and processing as outlined above, the data were accumulated into seasonal [MAM, June–August (JJA), September–November (SON), and DJF] and annual diurnal totals for each of the seven study years. This allowed the mean seasonal and annual diurnal rainfall cycles to be calculated for each year, as well as the mean annual and seasonal diurnal cycles, which are used in this study. A number of changes in the ECMWF model occurred during the study period, including a new cloud scheme in November 2010. However, a major new convection parameterization scheme was implemented in November 2007; consequently, the study period is divided into two 3-yr periods, March 2004 through February 2007 and March 2008 through February 2011, to facilitate the analysis of the impact of the new convection parameterization scheme.

4. Results

This section presents the analysis and interpretation of the comparison between the ECMWF operational forecast model and the two satellite-derived precipitation products.

a. Characteristics of model-derived precipitation

A comparison of the first 24-h with the second 24-h forecast period of the ECMWF model is shown in Fig. 1 for the periods covering the old and new convection schemes. It is clear that the model generates substantially more precipitation at the beginning of the forecast period with a mean difference of about 0.7 mm day^{-1} in the mean global tropical precipitation; this represents an increase of about 20% of the daily rainfall and relates to the spindown period of the model. While the new scheme reduces the initial peak difference, the 0–24 to 24–48-h differences are high for the 2–4 forecast periods, before becoming less once more. If the differences between the 0–24 and the 24–48-h forecasts are mapped (see Fig. 2), it can be seen that the model is generally "wet" (blue regions) in the first 24-h period, although this is not evenly distributed. The region along the ITCZ is the primary focus for this wet zone, with

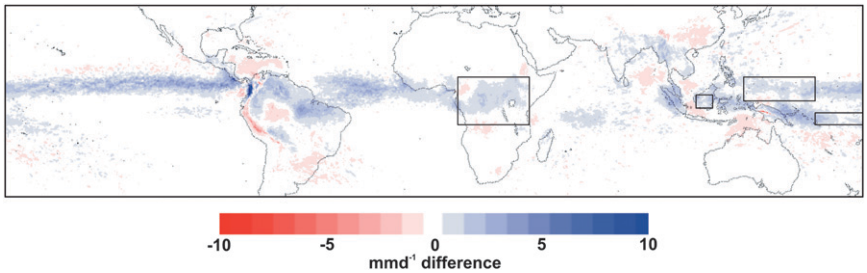

FIG. 2. Map of mean spindown differences, computed as the 24–28 h minus the initial 00–24-h precipitation forecast for March 2004 to February 2011. Rectangular boxes represent the regions used in the analysis, defined (from left to right) as central Africa (10°–40°E, 10°N–10°S), Borneo (110°–117°E, 2.5°N–3°S), western Pacific (130°–160°E, 10°N–0°), and SPCZ (160°E–180°, 5°–20°S).

regions just outside the ITCZ, along the Andes, and in South America showing less precipitation in the initial 24-h forecast periods. Outside of the tropics (between about 20°N–20°S), there are only small changes in the forecast precipitation between the two periods, suggesting that the spindown is largely related to the convection scheme within the model. However, the difference in daily means mask subdaily variations (not shown), where the 0–24 versus 24–48-h differences are particularly marked. In addition, seasonal differences have also been noted, in particular in the location of the ITCZ, which shifts southward during MAM in the later 24–48 forecast period compared with the initial 0–24-h period.

In addition to the differences between the initial and subsequent 24-h forecast periods, the modification of the convection parameterization scheme in the forecast model had the overall result of reducing the total precipitation in the tropics. This is illustrated in Fig. 3, which shows the latitudinal cross section for the two ECMWF parameterizations together with the TMPA and TRMM PR precipitation products. While the old ECMWF scheme generates up to 8 mm day^{-1}, the peak precipitation of the new scheme drops to less than 7 mm day^{-1} in the tropics. The new convection scheme produces precipitation amounts very much in agreement with the TMPA product between 5°N and 25°N; poleward of 15°S and 27°N, the old and new schemes generate approximately the same precipitation.

Although the amplitude of the daily maxima differs, analysis shows that the timing of the diurnal maxima does not appear to be affected by the change in the convection parameterization (Fig. 4). Over central Africa there appears to be little change in the precipitation between the pre- and postimplementation of the new convection scheme, with both the timing and the amounts being similar. Over Borneo, however, there has been a significant increase in precipitation of about 75% from about 11 mm day^{-1} to about 19 mm day^{-1} for the 0–24-h forecast and a similar increase for the 24–48-h forecast. The peak precipitation has also shifted later by about 1.5 h. Over the oceans, the SPCZ study area reveals a decrease in precipitation of about 2 mm day^{-1} due to the new convection scheme during the second period, although with little change in the phase. Over

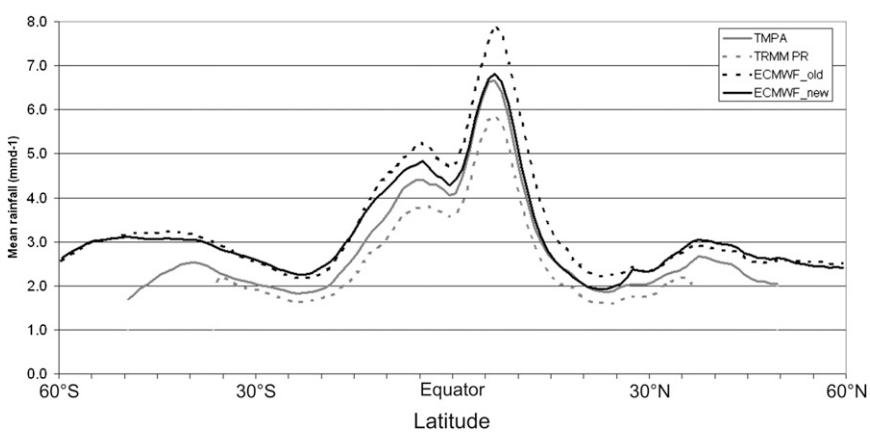

FIG. 3. Latitudinal cross section of the satellite (TMPA and TRMM PR) precipitation estimates together with the modeled estimates for the old and new convection schemes.

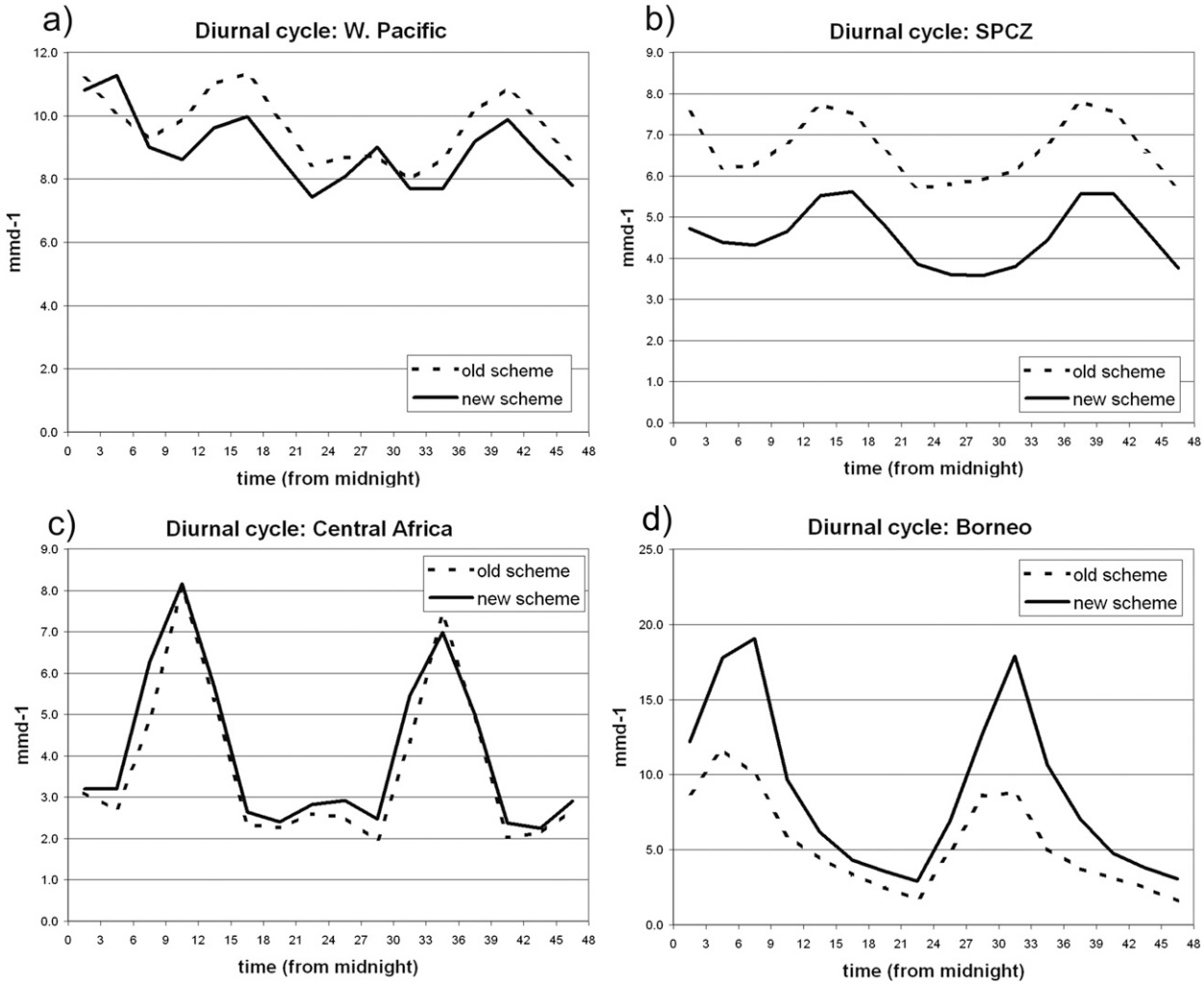

FIG. 4. Plots of comparison between the ECMWF old and new convection parameterization schemes; old parameterization scheme covers 2004–07 and the new parameterization scheme covers 2008–11 for (a) the western Pacific, (b) SPCZ, (c) central Africa, and (d) Borneo.

the western Pacific, the differences are less, with a decrease of about 1 mm day^{-1} over a similar diurnal cycle.

b. *Seasonal accumulations and differences*

Figure 5 shows the mapped precipitation products for DJF 2008–11 after the implementation of the ECMWF new convection parameterization; the ECMWF product is an accumulation of the 24–48-h periods to avoid the spindown bias. Overall, the precipitation patterns in all three products are correctly located with similar magnitudes in the amounts, although subtle differences do occur.

1) LAND, DJF

Over South America, the ECMWF shows significantly more precipitation along the Andes than either the TMPA or TRMM PR products suggest. In addition, the extent of the precipitation maximum over the Amazon differs between the ECMWF and TMPA products, with the TMPA indicating a decrease in precipitation between the Amazon and the Andes. Over North America the products agree well in terms of the distribution, although the TMPA precipitation is lighter over northern Mexico and the southern United States and heavier over the southeastern United States with respect to the ECMWF product; the TRMM PR product shows much less precipitation over this region. The distribution of precipitation is similar over Africa, although the ECMWF shows more precipitation over central Africa and the TMPA produces a slightly greater area over the Ethiopian highlands. The reverse is true over Southeast Asia, particularly over China, where the ECMWF

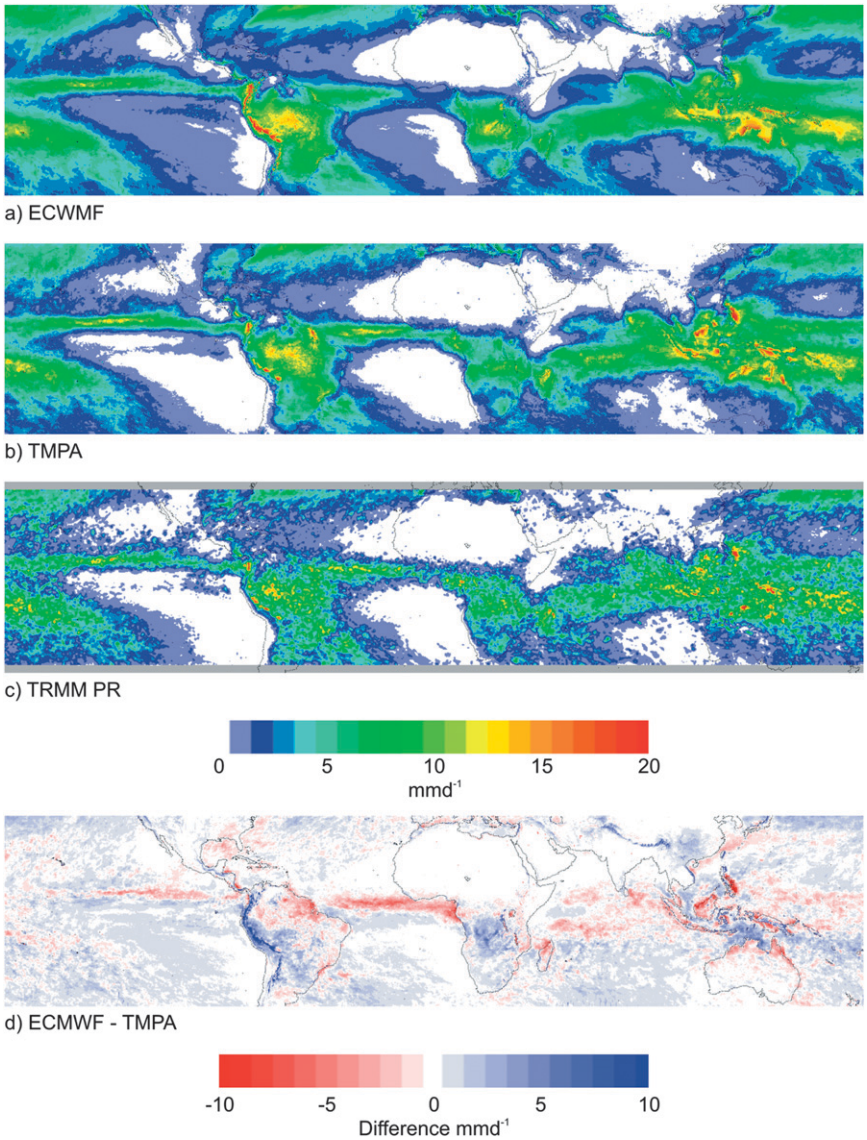

FIG. 5. Map of precipitation derived from (a) ECMWF, (b) TMPA, (c) TRMM PR, and (d) ECMWF minus TMPA for DJF 2008–11.

model generates more precipitation; the TMPA and TRMM PR products agree well in this area. Over Australia, all the products show similar distributions and amounts of precipitation.

2) OCEAN, DJF

Over the Pacific Ocean, the ECMWF generates more widespread precipitation than either the TMPA or TRMM PR products, with slightly more precipitation in the western Pacific to the northeast of Australia. In particular, the ECMWF generates more precipitation in the subtropical high-pressure regions to the west of South America and to the west of southern Africa. The peak intensity in precipitation along the ITCZ on the eastern Pacific differs; the ECMWF places this farther west than the TMPA product. In the tropical Atlantic the ECMWF and TMPA products differ in distribution and intensity; the ECMWF suggests a more westward bias in the distribution of precipitation while the TMPA suggests a minimum in precipitation close to the coast of South America and a more intense region of precipitation stretching across the Atlantic to the western coast of Africa, extending into the precipitation maximum over central Africa. Over the Indian Ocean the precipitation patterns are similar, although the TMPA product generates slightly more (about 1–2 mm day^{-1}) precipitation. Differences between the ECMWF and TMPA products can be seen around the East Indies, particularly over

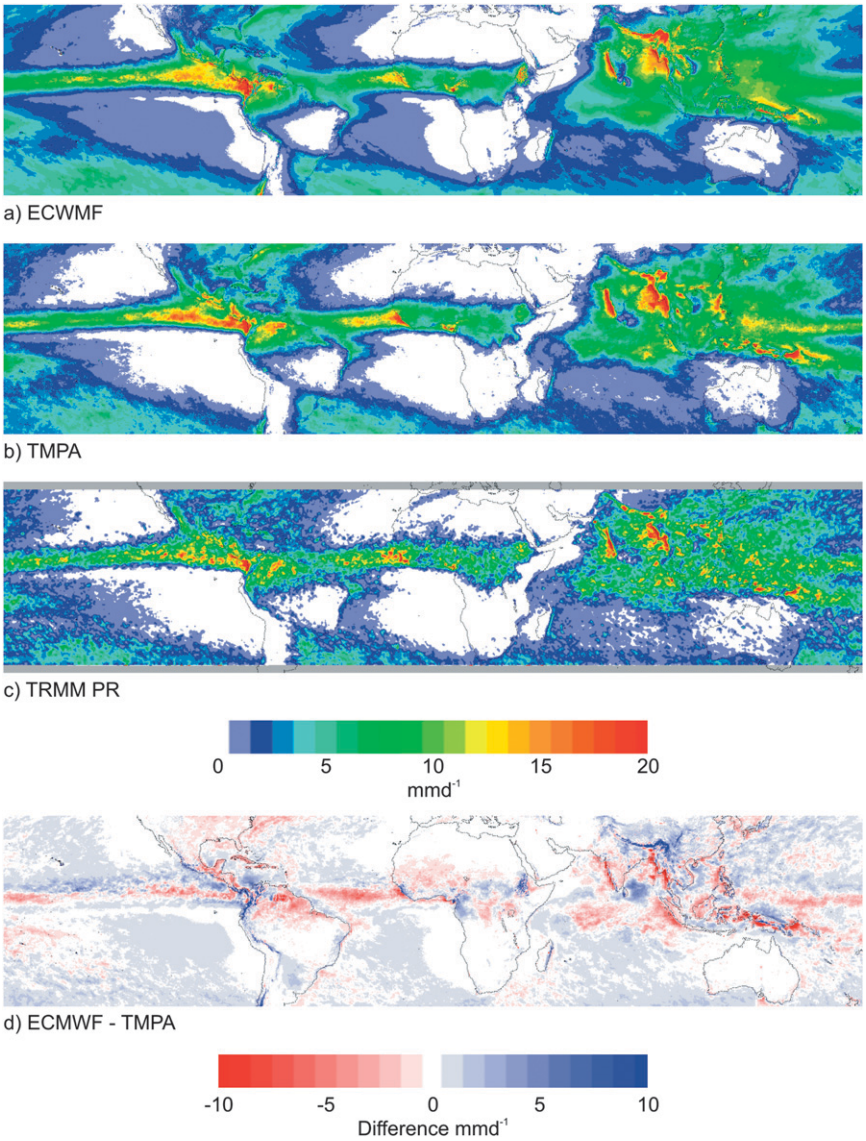

FIG. 6. As in Fig. 5, but for JJA 2008–11.

Borneo (ECMWF drier), between Borneo and Java, and over the Arafura Sea north of Australia (ECMWF wetter).

The differences between the ECMWF and TMPA precipitation products are summarized in Fig. 5d. The greatest differences are over the tropical Atlantic, northeastern Brazil, northern Australia, and over Borneo, where the ECMWF model is drier, and over the Andes, central Africa, Himalayan foothills, and Arafura Sea, where the ECMWF model is wetter.

The precipitation maps for JJA are shown in Fig. 6; the broad patterns between the three precipitation products are similar, although, as in the above period, the ECMWF model produces more precipitation in the subtropical high-pressure regions.

3) LAND, JJA

Over South America the precipitation is primarily over the northwest region, with the TMPA producing more precipitation, both in amount and extent, than the ECMWF; the ECMWF suggests an isolated maximum over the high ground of the Sierra Pacaraima in southern Venezuela. Over North America the TMPA product generates slightly more precipitation than the ECMWF over the U.S. Midwest and Southeast, although the amounts are generally small. The extent of precipitation over Africa is similar, with amounts of about 10 mm day^{-1}, although over the Ethiopian highlands the TMPA product suggests rainfall amounts no greater

than 10 mm day^{-1} while the ECMWF suggests isolated values in excess of 10 mm day^{-1}. Over the Indian subcontinent the distribution of rainfall is similar, although over the Himalayas the ECMWF model produces up to 10 mm day^{-1} more precipitation than the TMPA product (Fig. 6d).

4) OCEAN, JJA

Over the Pacific Ocean, the ECMWF model generates slightly more precipitation outside the tropics. Within the tropics the ECMWF places the ITCZ slightly north of the position of the ITCZ in the TMPA product, resulting in an ECMWF wet bias in the northern ITCZ region and dry bias to the south across the Pacific Ocean. Along the ITCZ in the tropical Atlantic, the precipitation in the ECMWF output is skewed to the east toward the coast of Africa while the TMPA and TRMM PR products suggest a more even distribution of precipitation with a maximum in the mid-Atlantic. In the Indian Ocean, the TMPA product produces a greater contrast between the precipitation minimum in the lee of Sri Lanka and the maxima further south. In addition, the TMPA and TRMM PR products suggest upwind enhancement off Sumatra, which is not shown in the model. Farther east over the East Indies, the ECMWF is drier over Borneo than the TMPA, and particularly so over New Britain.

c. *Time series analysis*

Figure 7 shows the time series analysis for the four regions shown in Fig. 2 for the whole period from March 2004 through February 2011. These are summarized below.

1) WESTERN PACIFIC

The three precipitation products are generally in good agreement across this region, although during 2005–07 the ECMWF model produced a wet bias while the TRMM PR product was drier than the TMPA. After the new convection parameterization in late 2007, the model product is very close to that of the TMPA, except for early in 2010.

2) SPCZ

All products suggest a general decreasing trend in precipitation over the 2004–11 period, with a particularly dry period in 2008. The ECMWF output is generally higher than the TMPA and TRMM PR products until late 2007, after which the ECMWF model agrees very well with the satellite estimates.

3) CENTRAL AFRICA

A semiannual cycle is observed in all precipitation products with similar magnitudes, although the ECMWF model tends to be wetter, particularly during the dry seasons identified by the TMPA and TRMM PR products. In contrast to the results over the ocean, the differences between the ECMWF and the TMPA product appear to be greater after the implementation of the new convection scheme.

4) BORNEO

Over this region there is more month-to-month variation, in part because of the smaller area being studied. Under the old convection scheme, the ECMWF model precipitation was significantly lower than the satellite estimates, while after the new convection scheme was implemented, agreement between the model and satellite products is much improved.

d. *Diurnal variations*

The precipitation generated by the satellite and model outputs over monthly and shorter time scales are generally in agreement down to the daily time scales. This relationship can be attributed to a number of factors; the model precipitation output is essentially constrained by other variables within the model, while the satellite precipitation is constrained through calibration with surface datasets. However, at subdaily temporal resolutions, both products are affected by cycles in precipitation that often provide a significant contribution to the daily totals.

Figure 8 presents the mapped differences between the TMPA and ECMWF precipitation estimates for four (out of the eight) 3-hourly subdaily periods; a negetive difference (ECMWF drier than TMPA) is depicted in red, while a positive difference (ECMWF wetter than TMPA) is depicted in blue. One of the striking features is the magnitude of the difference compared with those found between the monthly differences or the differences between the 0–24 and 24–48-h model runs (see Fig. 2). These maps indicate that, although there is good agreement at the daily scale, there is a substantial difference in the phase of the precipitation maxima at the subdaily time scale. These differences (up to 10 mm day^{-1}) are greatest over land and follow the solar cycle. For example, the ECMWF is wettest over New Guinea between 0000 and 0300 UTC, Sumatra and eastern Africa between 0600 and 0900 UTC, western Africa and Amazonia between 1200 and 1500 UTC, and western South America between 1800 and 2100 UTC. Conversely, the ECMWF output is drier over South America at 0000–0300 UTC, New Guinea and Borneo at 1200–1500 UTC, and Africa at 1800–2100 UTC. While certain artifacts are known to exist with the TMPA dataset, such as the retrieval of orographic precipitation (evidenced by an ECWMF wet bias along the Himalayas

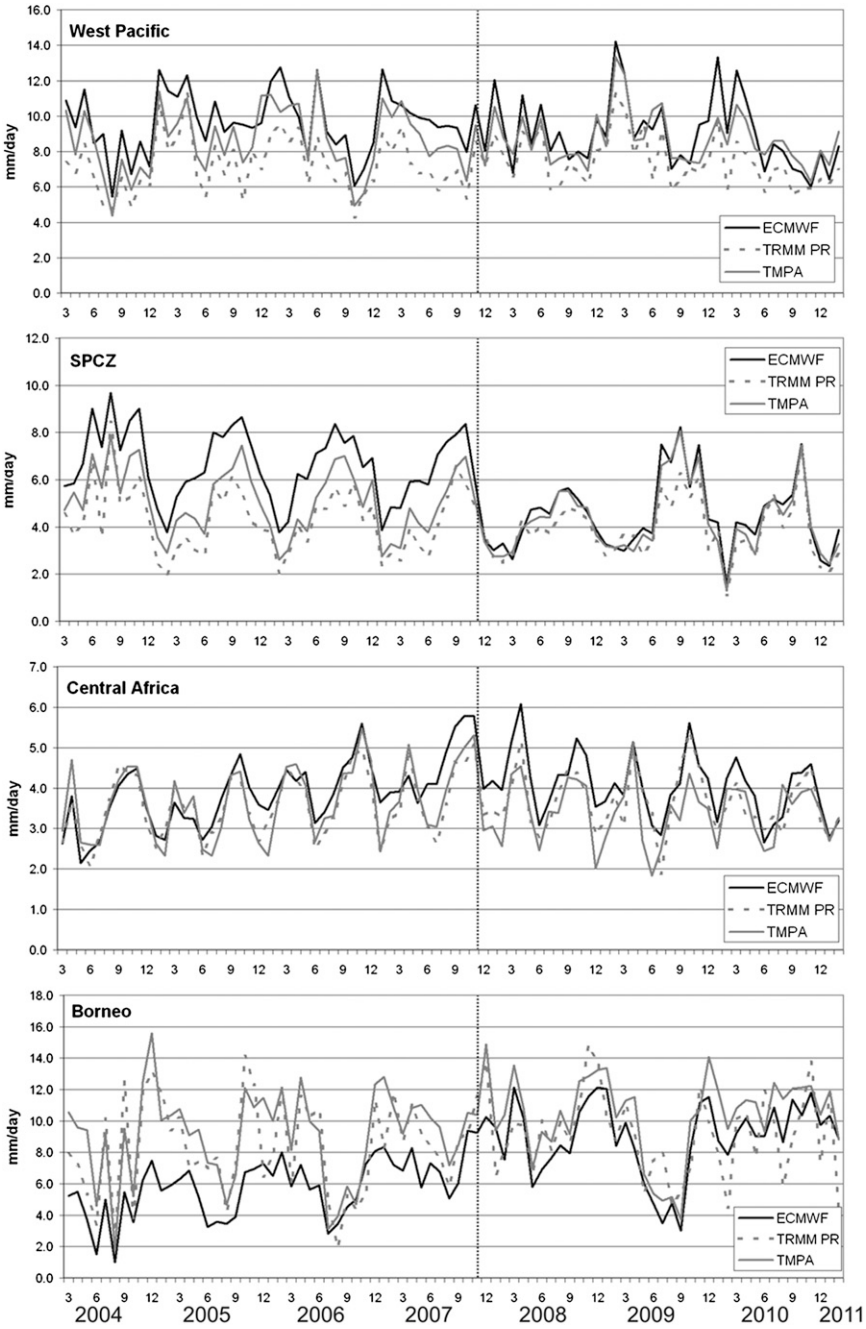

FIG. 7. Time series plots of monthly mean rainfall (mm day^{-1}) for the four selected regions (March 2004 to February 2011). The vertical dotted line marks the change in convection parameterization of the ECMWF model.

and the Andes), other broadscale differences and land–sea interactions tend to be more faithfully reproduced in the TMPA product.

Two regions of land–sea interactions stand out; the first is over Indonesia, and the other is along the northeast coast of Brazil. Over Indonesia at 0000–0300 UTC, there is a sharp land–sea contrast, with the ECMWF suggesting up to 10 mm day^{-1} more precipitation over the land areas compared with the TMPA, while conversely, around coastal seas of New Guinea, the ECMWF is up to 10 mm day^{-1} drier. These contrasts are reversed 12 h later, with the land regions being up to 10 mm day^{-1} drier in the model and the coastal seas up to 10 mm day^{-1} wetter. Over the northeast coast of

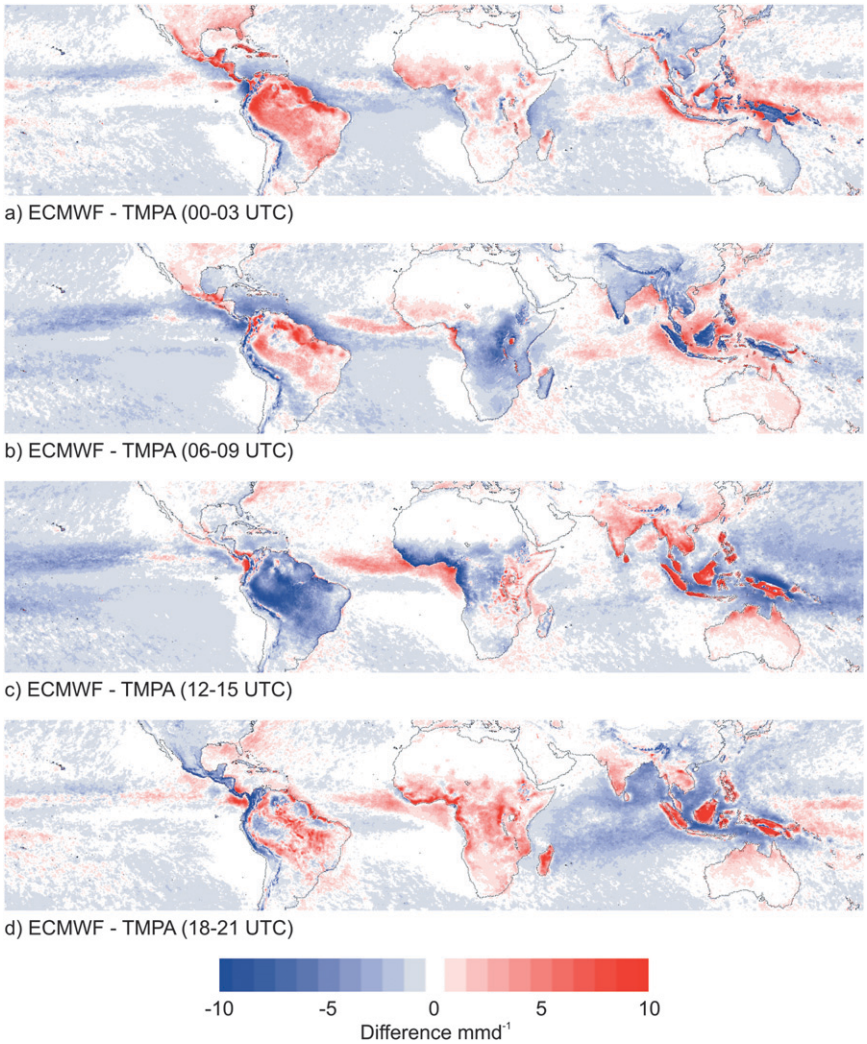

FIG. 8. Diurnal differences between the ECMWF and TMPA precipitation products for (top to bottom) 0000–0300, 0600–0900, 1200–1500, and 1800–2100 UTC during 2008–11. Blue (red) indicates ECMWF wetter (drier).

South America the situation is more complex; here the biases between the ECMWF and TMPA products lie parallel to the coast. At 0000–0300 UTC, the model is dry biased just inland of the coast, with a neutral–slightly positive bias farther inland and a dry bias over Amazonia; this situation continues through 0600–0900 UTC. From 1200–1500 UTC, the whole of South America is ECMWF wet biased. By 1800–2100 UTC, the biases are orientated along the coast, with the model dry biased along the coastal waters, wet biased just inland, then dry biased, wet biased, and finally dry biased close to the Andes. These features relate to known large-scale precipitation forcing in this region (see de Angelis et al. 2004) and will be discussed later.

The differences between the model and satellite estimates for the four regions are shown in Fig. 9 and are summarized below.

1) WESTERN PACIFIC

The timing between the ECMWF model and the satellite estimates is somewhat better during the 24–48-h period for the maximum precipitation, although the ECMWF leads the satellite estimates by about 1.5 h. The ECMWF also indicates a strong peak during the minimum precipitation in the 27–30-h forecast period; the TRMM PR product also suggests this, although with a smaller peak. Of note is the difference in the ECMWF model between 0–3 and 3–6 h and 24 h later between 24–27 and 27–30 h.

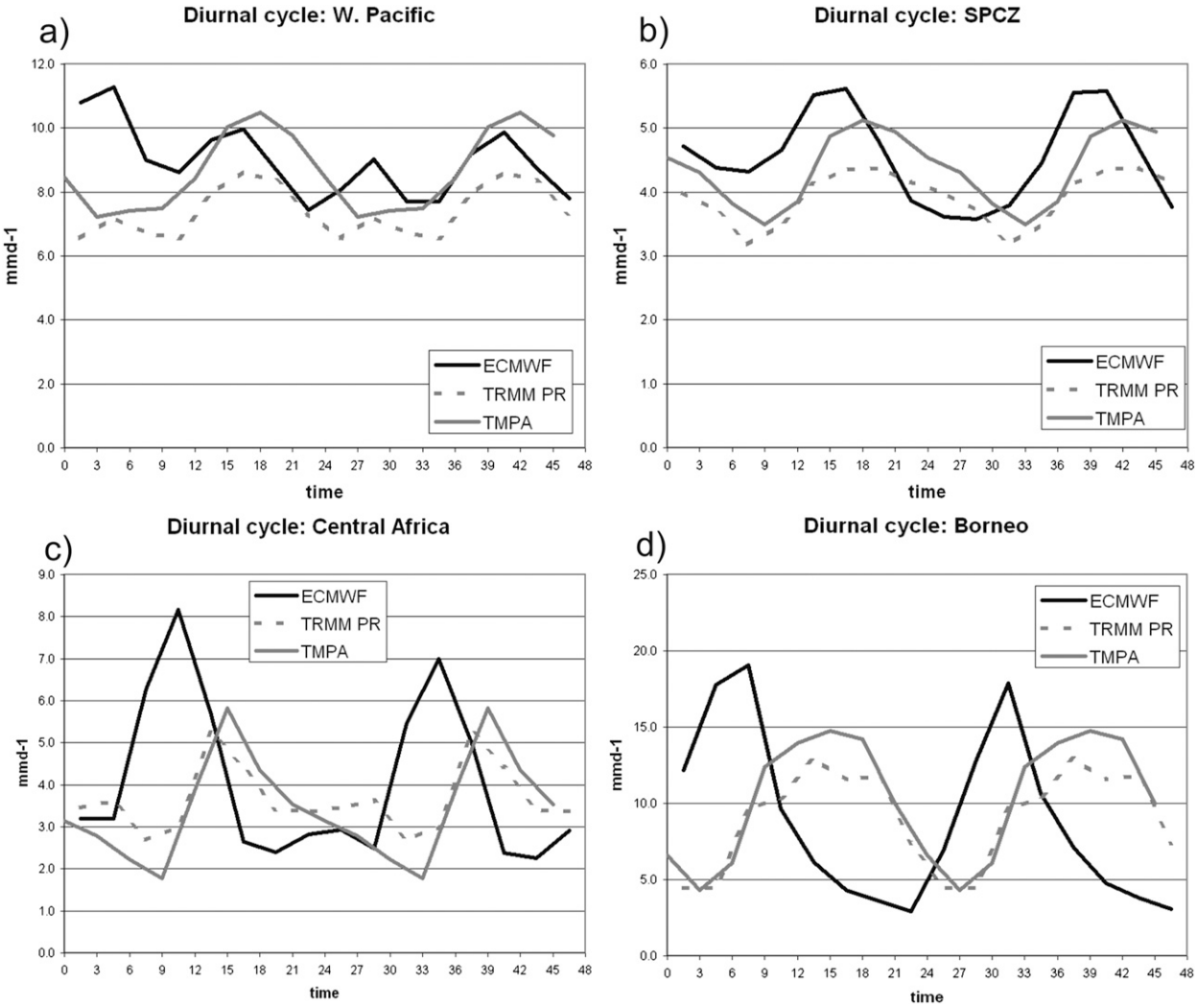

FIG. 9. Comparison plots of ECMWF, TRMM PR, and TMPA precipitation products over selected regions for the period 2008–11 for (a) western Pacific, (b) SPCZ, (c) central Africa, and (d) Borneo. Time on the *x* axis is the time from the start of the model forecast period.

2) SPCZ

Over the SPCZ, the ECMWF model maximum precipitation leads the TMPA and TRMM PR products by about 1.5 h, similar to that found over the western Pacific region. The peak rainfall is somewhat higher than the TMPA ($\sim$0.5 mm day^{-1}), and about 1 mm day^{-1} higher than the TRMM PR product. There is however a sharper drop-off in precipitation in the ECMWF model after the diurnal peak.

3) CENTRAL AFRICA

Over central Africa there is a striking diurnal cycle, particularly portrayed by the ECMWF model. The peak rainfall in the model leads the satellite estimates by about 3 h (TRMM PR) and 4.5 h (TMPA) and with a higher maximum of $\sim$8 mm day^{-1} (0–24 h) or $\sim$7 mm day^{-1} (24–48 h) compared with $\sim$6 mm day^{-1} in the TMPA product. Similar to the comparison over the SPCZ, the ECMWF also "rains out" more quickly than the satellite estimates suggest, while similar to the western Pacific region, the TRMM PR product suggests a small increase in precipitation just before the diurnal minimum, also depicted in the model.

4) BORNEO

The diurnal peak in the ECMWF model is, in this case, 6–9 h earlier and sharper than the satellite estimates would suggest. Both the TRMM PR and TMPA products are in agreement relating to the timing of the maxima, although the TRMM PR maximum rainfall is about 2 mm day^{-1} less than the TMPA amount.

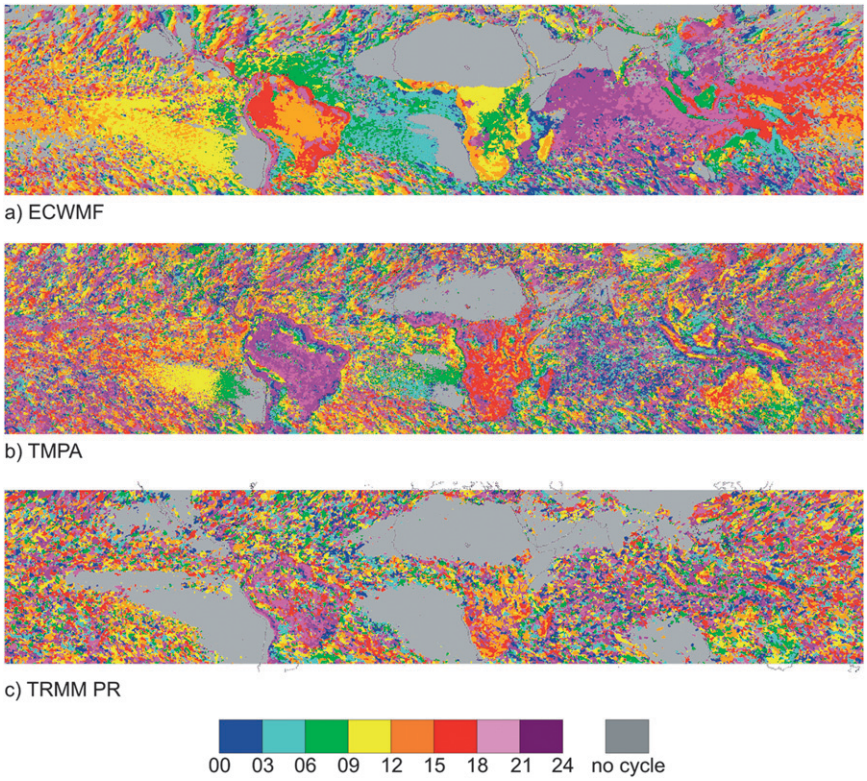

FIG. 10. Phase of maximum precipitation for DJF; times are in UTC: (a) ECWMF, (b) TMPA, and (c) TRMM PR. The gray shading indicates regions of no discernible diurnal cycle or mean precipitation less than 0.5 mm day^{-1}.

e. *Timing of precipitation maxima*

To elucidate the timing of the diurnal maxima, plots of the time (UTC) of the precipitation maximum for the ECMWF, TMPA, and TRMM PR products have been generated for DJF and JJA. Note that because of the poorer sampling of the TRMM PR, the PR images represent the whole period from 2004 to 2011 with a 3 × 3 weighted spatial filter applied, while the unfiltered ECMWF and TMPA products are for the period 2008–11. For clarity, only those grid boxes where the diurnal maximum contributed more than 15% of the rainfall with a minimum mean rainfall of 0.5 mm day^{-1} are shown.

The results for DJF are shown in Fig. 10. The ECMWF product shows broad areas of color, suggesting that the solar cycle has a significant influence on the generation of the peak daily precipitation, with the specific timing of the maximum being affected by land and sea background conditions. Over the Atlantic the maximum is generally between 0000 and 0900 UTC, in the eastern Pacific between 0600 and 1500 UTC, in the western Pacific between 1200 and 1800 UTC, and in the Indian Ocean between 1800 and 2400 UTC; these UTC times correspond to early morning local time. Over land, Africa experiences (an ECMWF) maxima between 0600 and 1500 UTC, South America between 1200 and 1800 UTC, and Southeast Asia between 1500 and 2400 UTC, relating to a morning through early afternoon local time. The map of diurnal maxima for the TMPA product is more varied, suggesting different timings for the maximum precipitation. Over the ocean the maxima are quite varied, except close to the subtropical high-pressure regions. In the Atlantic the maxima tend to be from 0600 to 1200 UTC, in the eastern Pacific from 1200 to 1800 UTC, in the western Pacific from 1500 to 2100 UTC, and in the Indian Ocean from 0000 to 0900 UTC (i.e., morning local time). Over land, Africa experiences its maxima almost entirely between 1500 and1800 UTC and South America between 1800 and 2400 UTC (although note the phase propagation inland away from the northeast coast), both afternoon/early evening local time. The TRMM PR product, although noisier, largely matches the timings of the TMPA maxima. Of particular note is that the ECMWF model tends to demarcate the land–sea regimes clearly, whereas the TMPA and TRMM PR suggest more complex land–sea interactions, particularly noticeable around Indonesia.

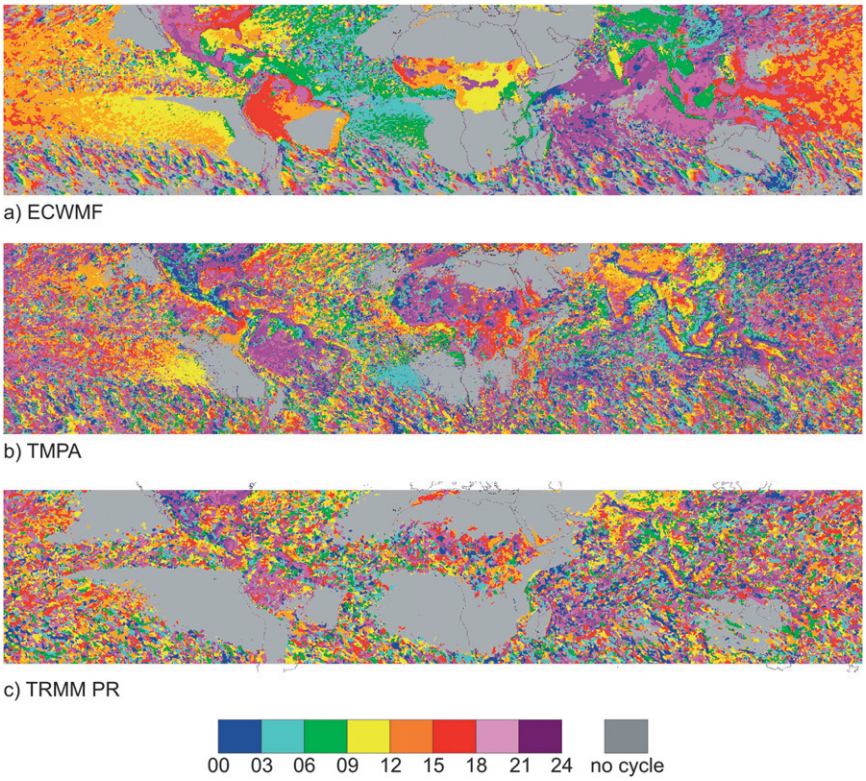

FIG. 11. As in Fig. 10, but for JJA.

Figure 11 shows the timings of the maxima for JJA and reflects the overall shift of the ITCZ northward. The timings of the maxima for all products and regions are similar to those in DJF. One difference is over the southeastern United States, where the ECMWF model suggests a maximum around 1500–1800 UTC (1000–1300 LT), extending to 1800–2100 UTC (1000–1300 LT) in the western United States. Over India and Southeast Asia the ECMWF produces peak precipitation between 0600 and 0900 UTC (1100–1400 LT) and 0900 and 1200 UTC (1600–1900 LT), respectively. Over these same regions the TMPA and TRMM PR products suggest the maxima occur between 2100 and 0300 UTC (1600–2200 LT) over the southeastern United States and between 0000 and 0900 UTC (1600–0300 LT) over the central and western United States, while the maxima over India are 1200–1800 UTC (1700–2300 LT) and over Southeast Asia are 0900–1800 UTC (1600–0100 LT).

5. Discussion

Through comparison of the ECMWF model output and the satellite products, it can be seen that the two different sources of precipitation information generally agree at the seasonal scale. At these temporal scales the differences are generally well constrained, mostly within a few millimeters per day, although notable differences occur over orographic regions (e.g., Andes in DJF and Himalayas in JJA, ECWMF wet bias) and over some oceanic regions (e.g., tropical Atlantic, ECMWF dry bias in DJF and JJA). However, across many regions, including Indonesia, central Africa, and South America, differences between the ECMWF model and the satellite products are evident at the subdaily scale. For example, over the ocean west of Mexico and Central America, the TMPA product demonstrates evidence of westward phase propagation moving away from the coastline, although these are absent in the ECMWF model. Such dynamics are most likely due to the occurrence of phase superposition resulting in enhanced amplitudes when phase of the propagating systems become coincident with the local diurnal maxima (Laing et al. 2008).

Phase superposition producing enhanced diurnal rainfall and a strong diurnal signal also appear to be found several hundred kilometers inland along the northwest coast of South America in the TMPA data (particularly DJF). This inland propagating rainband is well documented as a result of the land–sea breeze regime along the coastline (de Angelis et al. 2004). While the ECMWF model does appear to simulate some inland phase propagation close to the coast, it does not

exhibit the incursion of the large diurnal rainfall amplitudes that the TMPA depicts. This could be as a result of either incorrect simulation of local maxima along the landside coastline or incorrect characterization of the land–sea breeze.

Both the ECMWF model and TMPA data show similar distributions in the strength of the diurnal cycle, representing a relatively weak diurnal cycle ($<1.0\,\mathrm{mm\,day^{-1}}$) over open ocean areas with a stronger diurnal rainfall cycle over land and along the ITCZ, SPCZ, and other regions of strong convective activity. In addition, both the ECMWF model and TMPA products indicate differential timing of rainfall maxima for land and ocean areas, generally depicting morning maxima over ocean areas, although the exact timing differs. These results compare well with those found by other workers (Bechtold et al. 2004; Nesbitt and Zipser 2003; Sanderson et al. 2006; Liu et al. 2009; Takahashi et al. 2010; Vondou et al. 2010). Furthermore, the lowest relative errors between the ECMWF model and TMPA product tend to consistently occur over the majority of ocean areas throughout the diurnal cycle, indicating that the model reasonably well simulates the diurnal cycle over the open oceans.

While the ECMWF model demonstrates the same general diurnal rainfall characteristics over open ocean areas as those depicted by the TMPA estimate and other studies, they differ over land. These differences suggest that the ECMWF model is not characterizing the diurnal cycle over land well, where a late afternoon/early evening maxima is well documented (Yang and Slingo 2001; Kikuchi and Wang 2008; Liu et al. 2009; Vondou et al. 2010). The ECMWF model has a tendency to overestimate diurnal amplitude over the majority of land and ITCZ regions, relative to the TMPA estimates. This is corroborated by the findings of previous studies that have also shown that other models similarly tend to overestimate diurnal amplitudes over land areas, as well as along the SPCZ and west Indian Ocean (Bechtold et al. 2004; Neale and Slingo 2003; Lee et al. 2007; Shin et al. 2007; Wang et al. 2007). In contrast, the ECMWF model tends to underestimate diurnal amplitude over the majority of ocean areas relative to the TMPA data.

Over regions of high topography, such as the Ethiopian and Brazilian highlands, Himalayas, and the mountainous regions of India, Cameroon, and Nigeria, the ECMWF model tends to either underestimate or overestimate the diurnal rainfall amplitude (with respect to the satellite data); it exhibits a dry bias during JJA over Ethiopia and the mountainous regions of India, while showing a wet bias over the Andes. Such errors are likely to result from the inability of the model to correctly resolve highly variable subgrid orographic information resulting from a smoothing of the actual topography.

A close relationship exists between the diurnal amplitude and the timing of the diurnal rainfall maxima and orography, with distinct regional variability occurring as a result of differences in convection over highland and lowland regions. Indeed, Vondou et al. (2010) found that smaller amplitudes and near-midnight maxima tend to occur in lowland valley regions, while larger amplitudes and late afternoon maxima occur across highland regions. Liu et al. (2009) found similar nocturnal maxima around the periphery of the Tibetan Plateau, likely associated with the steep topography around the periphery resulting in strong localized mountain-valley breezes. Over the southern periphery of the Tibetan Plateau, the ECMWF model indicates some regions of late evening–early morning (2100–0300 LST) maxima, but this is several hours earlier than the TMPA, which is predominantly showing a 0300–0900 LST maxima.

The ECMWF model also appears to poorly represent the complex land–sea interactions, particularly noticeable around Indonesia. Studies have indicated that the correct representation of land–sea breezes is highly dependent on the horizontal resolution used (Ellis and Chen 2004; Wang et al. 2007; Sato et al. 2009), which is necessary to adequately resolve the coastal geometry and land–sea contrast (Baker et al. 2001; Zhu and Atkinson 2004; Wang et al. 2007). Land–sea breezes may also be affected by local topography because of strengthening near regions of high topography as a result of the influence of anabatic–upslope winds (Ellis and Chen 2004; Zhu and Atkinson 2004; Sato et al. 2009; Vondou et al. 2010), as well as the influence of vegetation cover and soil moisture (Baker et al. 2001; Miao et al. 2003). Further, it is thought that the sea breeze plays an important role in the initiation and maintenance of propagating convection in the landside coastal regime (Laing et al. 2008). Thus, the inadequate representation of the land sea breeze could result in the production of additional errors in the simulation.

For much of the tropics, the ECMWF model appears to simulate diurnal rainfall maxima too early relative to the TMPA and PR, leading by a few hours across the oceans but substantially more across land areas and the ITCZ region. This early bias has also been found by other studies using different models and observation estimates (Betts and Jakob 2002; Bechtold et al. 2004; Lee et al. 2007; Shin et al. 2007; Wang et al. 2007).

The TMPA and PR estimate depicts complex variations in the timing of the diurnal maxima (Figs. 10, 11), indicating the influence of small-scale local and regional

dynamics in the diurnal rainfall cycle, particularly along areas of land–sea contrast and regions of significant orographic variation. The TMPA also shows evidence of diurnal phase propagations away from the coastal regions of the Maritime Continent, West Africa, and the west coast of Mexico and South America. These results are supported by the findings of Yang and Slingo (2001), who also identified coherent phase propagations away from the coastal regions of the Maritime Continent, off the West African coast, within the Bay of Bengal, and southwestward off the Mexican coast.

The ECMWF model, in contrast, shows little of this complexity. Rather, it shows a greatly simplified variation in the timing of the diurnal maxima, together with poor representation of any phase propagations relative to the TMPA and PR. This is a key issue for the representation of large convective systems such as MCSs, which, although they only account for 10%–20% of all convective processes in the tropics, can contribute 70%–80% of the rainfall (Mohr et al. 1999; Laing et al. 2008) as well as much of the region's cloudiness; thus, it is important that they are adequately modeled.

While the diurnal rainfall variability is seasonally dependent over land and coastal regions in both the ECMWF model TMPA and PR datasets, little variation is seen across the oceans throughout the year. Over land, the diurnal variability increases (decreases) in the hemispheric summer (winter) season. This is most notable in the extratropics, where seasonal changes in insolation are most prominent.

The seasonal plots (Figs. 10, 11) generally show similar distributions in the timing of the diurnal rainfall maxima as those observed in the annual mean diurnal cycle plots for both datasets. Kikuchi and Wang (2008) found that, while the amplitude of the diurnal cycle was dependent on season (as a result of change in the amount of received insolation), the timing of the diurnal rainfall maxima was not. The results of this study largely support this assertion, with seasonal changes being clearly evident in the diurnal amplitude, but little change to the timing of the diurnal rainfall maxima. There are a number of possibilities that could explain the differences between the diurnal rainfall cycles depicted by the ECMWF model and TMPA estimate. As described previously, one problem with the ECMWF model in regions of high convective activity is likely due to the inadequate parameterizations of subgrid processes. Some errors may be attributed to the TMPA estimate. When no microwave information is available, the IR data are utilized; however, precipitation estimates derived from IR observations tend to lag behind surface precipitation because of the life cycle of convective cloud systems.

Differences between the performance of the ECMWF model over land and ocean areas provide support for different mechanisms in the production of the diurnal rainfall cycle. Over ocean, the diurnal rainfall cycle is much simpler, while over land, the diurnal rainfall cycle is often influenced by the complex interactions between numerous factors, such as orography, land–sea contrast, coastal geometry and the asymmetry between the strength of the land and sea breezes, and land surface cover, as well the initiation, persistence, and decay of mesoscale convective systems and gravity waves (Wang et al. 2007; Kikuchi and Wang 2008; Vondou et al. 2010). This complexity of the diurnal cycle over land means that, while the mechanisms of the diurnal cycle over land are well understood, the model performs better over the ocean areas.

All comparisons in this study of ECMWF model performance were made relative to the TRMM TMPA and TRMM PR products. Despite the TMPA generally performing well (Dai et al. 2007; Sapiano and Arkin 2009), it is possible that errors in the TMPA could have amplified or reduced real differences. It is therefore important to consider the influence of issues with the TMPA on the results of this study. The overall quality of the TMPA product does depend on the quality of the input data. As such, errors in the individual sensors can produce errors in the final TMPA product. The TMPA may also be biased low in regions of complex terrain because of gauge-location biases toward lower elevations. This general tendency to underestimate precipitation where the ECMWF has been shown to overestimate precipitation over land and along coastal regions could be enhancing this wet bias.

6. Conclusions

The ECMWF operational forecast model simulates diurnal rainfall maxima too early compared to the TMPA estimate, with the model appearing to be largely driven by the timing of the solar maximum insolation, as illustrated in Figs. 9–11. Over central Africa the model places the diurnal maximum 3–4 h ahead of the TMPA estimates, while overestimating the diurnal amplitude, by more than 30%. However, in regions of high topography, the model shows a dry bias and simulates the diurnal rainfall maxima too late. This is likely to be a result of not adequately resolving the complex subgrid-scale orographic detail within the model. The ECMWF model tends to show a very simplified diurnal cycle over the majority of areas, most notably the Maritime Continent.

While mechanisms producing the midafternoon to late evening rainfall maxima over land are well known,

the ECMWF model tends to better represent the diurnal rainfall cycle over open ocean areas where the causal mechanisms are less well known. The agreement between the ECMWF and satellite products over these regions is generally very good (see Fig. 7), which in itself is encouraging since oceanic regions are generally data-sparse regions. Over land areas the agreement between the model and satellite is less good and is likely to result from the strong regional forcing mechanisms on the diurnal cycle over and near land, which the ECMWF model simulates less well. The late afternoon–early evening peak in the precipitation over land observed in the satellite products is consistent with subdaily rain gauge observations.

The ECMWF model tends to show a dry bias on the seaward coastal regions under the influence of land–sea breezes and a wet bias along the corresponding landside coastal region relative to the TMPA. Exceptions to this do exist though, such as along the northern South American coast, which provide support for the diurnal rainfall cycle being complex and influenced by a combination of many separate factors. A model must adequately represent these if it is to successfully model the diurnal rainfall cycle.

Acknowledgments. The authors acknowledge the support of the U.K. Natural Environment Research Council through their Master Training Grant (NE/H525454/1), which supported the second author. Thanks also go to the European Centre for Medium-Range Weather Forecasts for provision of their operational forecast precipitation product and to NASA's Precipitation Processing System for the TMPA and PR datasets. We would also like to thank the anonymous reviewers for their diligence in reviewing the manuscript.

REFERENCES

Allan, R. P., B. J. Soden, V. O. John, W. Ingram, and P. Good, 2010: Current changes in tropical precipitation. *Environ. Res. Lett.,* **5,** 025205, doi:10.1088/1748-9326/5/2/025205.

Aonashi, K., and Coauthors, 2009: GSMaP passive, microwave precipitation retrieval algorithm: Algorithm description and validation. *J. Meteor. Soc. Japan,* **87A,** 119–136.

Baker, R. D., B. H. Lynn, A. Boone, T. Wei-Kuo, and J. Simpson, 2001: The influence of soil moisture, coastline curvature, and land-breeze circulations on sea-breeze-initiated precipitation. *J. Hydrometeor.,* **2,** 193–211.

Bauer, P., E. Moreau, and S. Di Michele, 2005: Hydrometeor retrieval accuracy using microwave window and sounding channel observations. *J. Appl. Meteor.,* **44,** 1016–1032.

Bechtold, P., J.-P. Chaboureau, A. Beljaars, A. K. Betts, M. Köhler, M. Miller, and J.-L. Redelsperger, 2004: The simulation of the diurnal cycle of convective precipitation over land in a global model. *Quart. J. Roy. Meteor. Soc.,* **130,** 3119–3137, doi:10.1256/qj.03.103.

Bell, T. L., and N. Reid, 1993: Detecting the diurnal cycle of rainfall using satellite observations. *J. Appl. Meteor.,* **32,** 311–322.

Betts, A. K., and C. Jakob, 2002: Evaluation of the diurnal cycle of precipitation, surface thermodynamics and surface fluxes in the ECMWF model using LBA data. *J. Geophys. Res.,* **107,** 8045, doi:10.1029/2001JD000427.

Bridgman, H. A., and J. E. Oliver, 2006: *The Global Climate Systems: Patterns, Processes, and Teleconnections.* Cambridge University Press, 350 pp.

Dai, A., F. Giorgi, and K. E. Trenberth, 1999: Observed and model-simulated diurnal cycles of precipitation over the contiguous United States. *J. Geophys. Res.,* **104** (D6), 6377–6402.

——, X. Lin, and K.-L. Hsu, 2007: The frequency, intensity, and diurnal cycle of precipitation in surface and satellite observations over low- and mid-latitudes. *Climate Dyn.,* **29,** 727–744.

de Angelis, C. F., G. R. McGregor, and C. Kidd, 2004: A 3 year climatology of rainfall characteristics over tropical and subtropical South America based on Tropical Rainfall Measuring Mission Precipitation Radar data. *Int. J. Climatol.,* **24,** 385–399.

Ebert, E. E., J. E. Janowiak, and C. Kidd, 2007: Comparison of near real-time precipitation estimates from satellite observations and numerical models. *Bull. Amer. Meteor. Soc.,* **88,** 47–64.

Ellis, R. T., and S. S. Chen, 2004: Effects of sea breeze and local winds on rainfall in south Florida. Preprints, *26th Conf. on Hurricanes and Tropical Meteorology,* Miami, FL, Amer. Meteor. Soc., 13B.2. [Available online at https://ams.confex.com/ams/pdfpapers/75846.pdf.]

Gray, W. M., and R. W. Jacobsen, 1977: Diurnal variation of deep cumulus convection. *Mon. Wea. Rev.,* **105,** 1171–1188.

Huffman, G. J., R. F. Adler, D. T. Bolvin, and E. J. Nelkin, 2010: The TRMM Multi-Satellite Precipitation Analysis (TMPA). *Satellite Rainfall Applications for Surface Hydrology,* M. Gebremichael and F. Hossain, Eds., Springer, 3–22.

Iguchi, T., and R. Meneghini, 1994: Intercomparison of single-frequency methods for retrieving a vertical rain profile from airborne or spaceborne radar data. *J. Atmos. Oceanic Technol.,* **11,** 1507–1516.

——, T. Kozu, J. Kwiatkowski, R. Meneghini, J. Awaka, and K. Okamoto, 2009: Uncertainties in the rain profiling algorithm for the TRMM Precipitation Radar. *J. Meteor. Soc. Japan,* **87A,** 1–30, doi:10.2151/jmsj.87A.1.

Joyce, R. J., J. E. Janowiak, P. A. Arkin, and P. Xie, 2004: CMORPH: A method that produces global precipitation estimates from passive microwave and infrared data at high spatial and temporal resolution. *J. Hydrometeor.,* **5,** 487–503.

Jung, T., and Coauthors, 2010: The ECMWF model climate: Recent progress through improved physical parametrizations. *Quart. J. Roy. Meteor. Soc.,* **136,** 1145–1160, doi:10.1002/qj.634.

Kalnay, E., 2003: Historical overview of numerical weather prediction. *Handbook of Weather, Climate, and Water: Dynamics, Climate, Physical Meteorology, Weather Systems, and Measurements,* T. D. Potter and B. R. Colman, John Wiley & Sons, Inc., 95–115.

Kelly, G. A., P. Bauer, A. J. Geer, P. Lopez, and J. N. Thepaut, 2008: Impact of SSM/I observations related to moisture, clouds, and precipitation on global NWP forecast skill. *Mon. Wea. Rev.,* **136,** 2713–2726.

Kidd, C., and G. Huffman, 2011: Global precipitation measurement. *Meteor. Appl.,* **18,** 334–353, doi:10.1002/met.284.

——, and V. Levizzani, 2011: Status of satellite precipitation retrievals. *Hydrol. Earth Syst. Sci. Discuss.,* **15,** 1109–1116, doi:10.5194/hess-15-1109-2011.

——, ——, and P. Bauer, 2009: Remote sensing of meteorology and climatology. *Prog. Phys. Geogr.,* **33,** 474–489.

——, P. Bauer, J. Turk, G. J. Huffman, R. Joyce, K.-L. Hsu, and D. Braithwaite, 2012: Inter-comparison of high-resolution precipitation products over northwest Europe. *J. Hydrometeor.,* **13,** 67–83.

Kikuchi, K., and B. Wang, 2008: Diurnal precipitation regimes in the global tropics. *J. Climate,* **21,** 2680–2696.

Kubota, H., and T. Nitta, 2001: Diurnal variations of tropical convection observed during the TOGA-COARE. *J. Meteor. Soc. Japan,* **79,** 815–830, doi:10.2151/jmsj.79.815.

Kummerow, C., W. Barnes, T. Kozu, J. Shiue, and J. Simpson, 1998: The Tropical Rainfall Measuring Mission (TRMM) sensor package. *J. Atmos. Oceanic Technol.,* **15,** 809–816.

Laing, A. G., R. Carbone, V. Levizzani, and J. Tuttle, 2008: The propagation and diurnal cycles of deep convection in northern tropical Africa. *Quart. J. Roy. Meteor. Soc.,* **134A,** 93–109.

Lee, M.-I., S. D. Schubert, M. J. Suarez, T. L. Bell, and K.-M. Kim, 2007: Diurnal cycle of precipitation in the NASA Seasonal to Interannual Prediction Project atmospheric general circulation model. *J. Geophys. Res.,* **112,** D16111, doi:10.1029/2006JD008346.

Liu, C. H., and M. W. Moncrieff, 1998: A numerical study of the diurnal cycle of tropical oceanic convection. *J. Atmos. Sci.,* **55,** 2329–2344.

Liu, X., A. Bai, and C. Liu, 2009: Diurnal variations of summertime precipitation over the Tibetan Plateau in relation to orographically-induced regional circulations. *Environ. Res. Lett.,* **4,** 045203, doi:10.1088/1748-9326/4/4/045203.

Mahfouf, J. F., P. Bauer, and V. Marecal, 2005: The assimilation of SSM/I and TMI rainfall rates in the ECMWF 4D-Var system. *Quart. J. Roy. Meteor. Soc.,* **131,** 437–458, doi:10.1256/qj.04.17.

McGuffie, K., and A. Henderson-Sellers, 2005: *A Climate Modelling Primer.* 3rd Ed. John Wiley & Sons, 296 pp.

Meehl, G. A., and Coauthors, 2007: Global climate projections. *Climate Change 2007: The Physical Science Basis,* S. Solomon et al., Eds., Cambridge University Press, 747–845.

Miao, J. F., L. J. M. Kroon, J. V. G. de Arrelano, and A. A. M. Holtslag, 2003: Impacts of topography and land degradation on the sea breeze over eastern Spain. *Meteor. Atmos. Phys.,* **84,** 157–170, doi:10.1007/s00703-002-0579-1.

Michaelides, S., V. Levizzani, E. Anagnostou, P. Bauer, T. Kasparis, and J. E. Lane, 2009: Precipitation: Measurement, remote sensing, climatology and modelling. *Atmos. Res.,* **94,** 512–533.

Mohr, K. I., J. S. Famiglietti, and E. J. Zipser, 1999: The contribution to tropical rainfall with respect to convective system type, size, and intensity estimated from the 85-GHz ice-scattering signature. *J. Appl. Meteor.,* **38,** 596–606, doi:10.1175/1520-0450.

Moreau, E., P. Bauer, and F. Chevallier, 2003: Variational retrieval of rain profiles from spaceborne passive microwave radiance observations. *J. Geophys. Res.,* **108,** 4521, doi:10.1029/2002JD003315.

Neale, R., and J. Slingo, 2003: The maritime continent and its role in the global climate: A GCM study. *J. Climate,* **16,** 834–848.

Negri, A. J., T. L. Bell, and L. Xu, 2002: Sampling of the diurnal cycle of precipitation using TRMM. *J. Atmos. Oceanic Technol.,* **19,** 1333–1344.

Nesbitt, S. W., and A. M. Anders, 2009: Very high resolution precipitation climatologies from the Tropical Rainfall Measuring Mission precipitation radar. *Geophys. Res. Lett.,* **36,** L15815, doi:10.1029/2009GL038026.

——, and E. J. Zipser, 2003: The diurnal cycle of rainfall and convective intensity according to three years of TRMM measurements. *J. Climate,* **16,** 1456–1475.

New, M., M. Todd, M. Hulme, and P. Jones, 2001: Precipitation measurements and trends in the twentieth century. *Int. J. Climatol.,* **21,** 1899–1922.

Peixoto, J. S., and A. H. Oort, 1992: *Physics of Climate.* American Institute of Physics, 520 pp.

Sanderson, V. L., C. Kidd, and G. R. McGregor, 2006: A comparison of TRMM microwave techniques for detecting the diurnal rainfall cycle. *J. Hydrometeor.,* **7,** 687–704.

Sapiano, M. R. P., and P. A. Arkin, 2009: An intercomparison and validation of high-resolution satellite precipitation estimates with 3-hourly gauge data. *J. Hydrometeor.,* **10,** 149–166.

Sato, T., H. Miura, M. Satoh, Y. Takayabu, and Y. Wang, 2009: Diurnal cycle of precipitation in the tropics simulated in a global cloud-resolving model. *J. Climate,* **22,** 4809–4826.

Shin, D. W., S. Cocke, and T. E. LaRow, 2007: Diurnal cycle of precipitation in a climate model. *J. Geophys. Res.,* **112,** D13109, doi:10.1029/2006JD008333.

Takahashi, H. G., H. Fujinami, T. Yasanari, and J. Matsumoto, 2010: Diurnal rainfall pattern observed by Tropical Rainfall Measuring Mission Precipitation Radar (TRMM-PR) around the Indochina peninsula. *J. Geophys. Res.,* **115,** D07109, doi:10.1029/2009JD012155.

Tompkins, A. M., and F. Di Giuseppe, 2010: Cloud radiative interactions and their uncertainty in climate models. *Stochastic Physics and Climate Modelling,* T. Palmer and P. Williams, Eds., Cambridge University Press, 327–374.

Trenberth, K. E., 1991: Climate diagnostics from global analyses: Conservation of mass in ECMWF analysis. *J. Climate,* **4,** 707–722.

Vondou, D. A., A. Nzeukou, A. Lenouo, and F. M. Kamga, 2010: Seasonal variations in the diurnal patterns of convection in Cameroon–Nigeria and the neighboring areas. *Atmos. Sci. Lett.,* **11,** 290–300, doi:10.1002/asl.297.

Wang, Y., L. Zhou, and K. Hamilton, 2007: Effect of convective entrainment/detrainment on the simulation of the tropical precipitation diurnal cycle. *Mon. Wea. Rev.,* **135,** 567–583.

Yang, G.-Y., and J. Slingo, 2001: The diurnal cycle in the tropics. *Mon. Wea. Rev.,* **129,** 784–801.

Yang, S., and E. A. Smith, 2005: Resolving SSM/I–ship radar rainfall discrepancies from AIP-3. *Adv. Atmos. Sci.,* **22,** 903–914. doi:10.1007/BF02918689.

Zhu, M., and B. W. Atkinson, 2004: Observed and modelled climatology of the land-sea breeze circulation over the Persian Gulf. *Int. J. Climatol.,* **27,** 883–905.